ELSEVIER

Journal of Membrane Science 93 (1994) 209–215

journal of MEMBRANE SCIENCE

Structural study of microporous polypropylene hollow fiber membranes made by the melt-spinning and cold-stretching method

Jae-Jin Kim[a,*], Tae-Seok Jang[a], Young-Don Kwon[a], Un Young Kim[a], Sung Soo Kim[b]

[a]*Membrane Laboratory, Korea Institute of Science and Technology, P.O. Box 131, Cheongryang, Seoul, South Korea*
[b]*Department of Chemical Engineering, Kyung Hee University, Seoul, South Korea*

Received 10 February 1992; accepted in revised form 14 March 1994

Abstract

Microporous polypropylene hollow fiber membranes were prepared by the melt-spinning and cold-stretching method. Factors affecting the membrane structure were melt-draw ratio, spinning temperature, and annealing temperature. The degree of molecular orientation was affected by the melt-draw ratio and spinning temperature, and the crystallinity of the hollow fiber depended on the melt-draw ratio and annealing temperature. Quantitative analyses of microporous membrane structure were performed by image analysis, bubble point pressure measurement, and mercury porosimetry. The porosity at the surface is smaller than that of the whole membrane. Wetting of the medium and shading in the image brought about the differences in pore size determination by each method.

Keywords: Microporous membranes; Membrane formation; Membrane pore size; Membrane porosity; Hollow fiber; Cold-stretching; Microcrystalline lamella

1. Introduction

Semicrystalline polymer such as polypropylene (PP) and polyethylene (PE) have been utilized for the preparation of the microporous membranes. Thermally-induced phase separation (TIPS) [1,2] and melt-spinning (or extrusion for flat membranes) and cold-stretching (MSCS) [3,4] techniques are generally used for this purpose. The micropore formation mechanism of each process is totally different. In the TIPS process, the sample is comprised of a polymer and diluent, which form a homogeneous melt above its melting temperature. Then it undergoes solid–liquid or liquid–liquid phase separation upon cooling. The sites occupied by the diluent become micropores after removal of the diluent. In the MSCS process, a pure polymer melt is spun, and the micropores are formed by the mechanical force acting on the membranes in a subsequent cold-stretching step. Therefore, the MSCS process does not involve any phase separation, and its handling is relatively easy.

In the TIPS process, the pore size can be controlled by adjusting the cooling condition, and by selecting appropriate diluents. In the MSCS process, pore size control is not as easy as in the TIPS process. However, installation of a coagulation bath and extraction of diluent are required in the TIPS process, and it results in waste solvent problems. The MSCS process is much simpler than the TIPS process in this respect, and has ad-

*Corresponding author.

SSDI 0376-7388(94)00070-F

vantages over the other processes in terms of mass production.

A melt extrusion and cold-drawing technique to make microporous flat membranes was first proposed by the Celanese Corporation in 1974 [5]. However, these membranes were not successful in terms of water flux when compared with the conventional cellulose acetate membranes. The Mitsubishi Corporation changed the configuration of the membranes to a hollow fiber type via the MSCS process in 1977, and they attained a remarkable increase in water flux to commercialize the membranes [3]. Besides its present use for blood oxygenators [6], it is gaining use in other applications, such as desalination, ultra-pure water preparation, and biosensors [7].

The micropore formation mechanism via MSCS is related to the microcrystalline lamellae which are in turn aligned in rows parallel to the extrusion direction [8]. This structure largely occurs by the high stress during the extrusion process and is completed during annealing. This type of morphology is reported by Keller and Marchin and referred to as a *row lamellar structure* [9]. Micropore formation results from the lamellae spreading during the cold-stretching process. Therefore, the pore size and its distribution are dependent on structural properties such as crystallinity and degree of orientation of the hollow fiber before cold-stretching.

In this study, PP hollow fiber membranes were prepared via the MSCS process, and the factors affecting the membrane structure were examined in terms of crystallinity and degree of molecular orientation. Pore size distribution and porosity of the hollow fiber membranes were determined by image analysis, bubble point pressure measurement, and mercury porosimetry. Data obtained from each method have been compared and explained in terms of the characteristics of each method.

2. Experimental

2.1. Materials and apparatus

Fiber grade isotactic PP (#5016H) was obtained from Dae-Han Yuhwa Co., South Korea, and its weight average molecular weight is 200,000 and melt index is 15 g/10 min.

A melt-spinning system was designed as shown in Fig. 1. A single-hole tube-in-orifice type spinneret was manufactured with inner and outer diameters of 9 and 10 mm, respectively, and a L/D ratio of 1.6. A gear pump supplied by Kawasaki Co., Japan (KHP-1H-0.3) was installed for exact metering of the melt to the spinneret. Hollow cross sections were formed by nitrogen being fed through the melt. A counter-current type air quencher was installed for effective cooling of the spun fiber. Installing double screens between the spinneret and air quencher helped maintain constant melt temperature by blocking the cooling air stream from the air quencher to the spinneret.

2.2. Formation of membranes

The procedure to prepare PP hollow fiber membranes is described in Fig. 2. The spinning temperature was varied between 180 and 230°C, and the cooling distance from the spinneret to

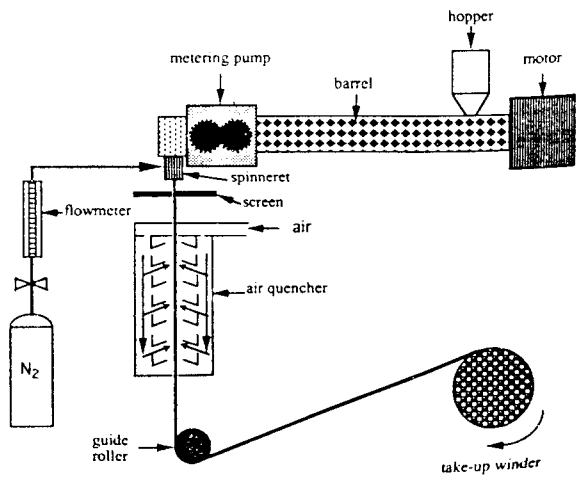

Fig. 1. Hollow fiber spinning apparatus.

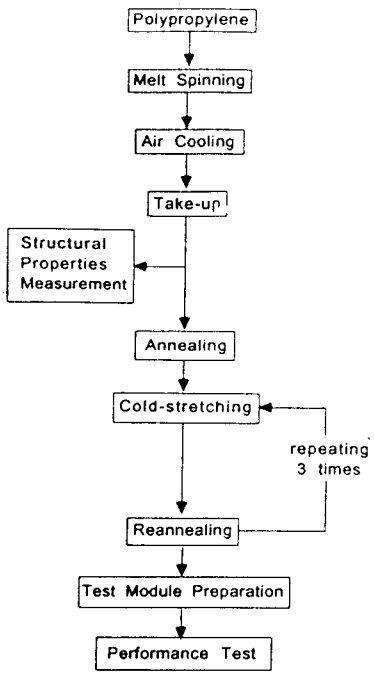

Fig. 2. Microporous polypropylene hollow fiber membrane preparation procedure.

the guide roller was set to 0.6 m. The melt-draw ratio of the spun fiber was defined as:

$$\text{Melt-draw ratio} = \text{Take-up speed/Extrusion rate} \quad (1)$$

and was controlled by adjusting the take-up speed with a constant extrusion rate of 76.6 cm/min. The extrusion rate is the linear velocity of the spun fiber coming out from the spinneret and was calculated from the ratio of the amount of melt fed to the spinneret to the annular cross-sectional area of the spinneret.

The hollow fibers were subsequently annealed at 60–140°C for 30 min to increase crystallinity. Then the hollow fibers were cold-stretched at room temperature to form micropores, and reannealed at 150°C for 1 min. The cold-stretching and reannealing steps were repeated 3 times with a cold-stretching ratio of 30, 30, and 50% (154% total stretch ratio).

2.3. Structure analysis and performance test

Birefringence of each hollow fiber membrane was measured by a polarization microscope (Nikon, Optiphot-pol HFX-IIA). The density of each hollow fiber membrane was measured at 23°C using a density gradient column filled with an ethanol–water mixture according to the ASTM D151-85 specification. The bubble point pressure of the hollow fiber membrane was measured using the apparatus shown in Fig. 3 according to the ASTM F 316-80 and E 12-61 specifications. The medium in the bath was an ethanol–water mixture (30 vol% of ethanol) to overcome the hydrophobicity of the PP membrane. The maximum pore size (D_{max}) of the hollow fiber membrane was calculated using

$$D_{max} = (4\gamma \cos\theta)/P \quad (2)$$

where γ is the surface tension, θ is the contact angle, and P is the bubble point pressure. Since Eq. (2) is the formula for cylindrical pore size determination, it does not exactly represent the size of the tortuous pores as formed in this study.

The structures of the inner and outer surfaces of the hollow fiber membranes were examined using a scanning electron microscope (Akashi Seisakusho Ltd., ISI DS 130). The images obtained from scanning electron microscopy were used to determine the pore size and pore size distributions at both membrane surfaces by using an image analyzer (Bausch & Lomb Co., Omicon 3500).

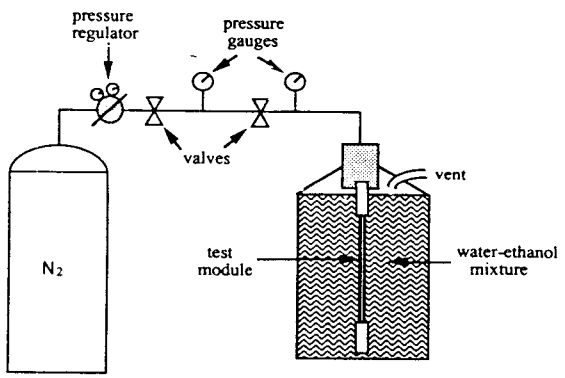

Fig. 3. Bubble point pressure test apparatus.

The porosity and pore size of the membrane were measured using a mercury porosimeter. A weighed amount of hollow fiber membrane was introduced into the chamber filled with mercury. Then the pressure was increased to fill the micropores of the membrane with mercury. By monitoring the volume change of mercury and the corresponding pressure, the pore size and porosity of the membrane were obtained [10].

3. Results and discussion

Melt-draw ratio, spinneret temperature, and annealing temperature are important factors influencing the membrane structure and performance. These factors influence the crystallinity and the degree of orientation of the hollow fibers. As shown in Fig. 4a, birefringence increased with increasing melt-draw ratio, i.e., a larger degree of molecular orientation of the hollow fiber. Since the viscosity of the polymer melt increased with decreasing temperature, the stress on the polymer melt increased while it passed through the spinneret resulting in an increase in the degree of orientation of the hollow fiber. Therefore, the hollow fibers spun at lower temperature have greater birefringence than those spun at higher temperature (Fig. 5a). However, birefringence of the hollow fiber was not affected by the annealing step as shown in Fig. 6a, since annealing had no influence on the orientation of the hollow fibers.

The crystallinity of the hollow fiber membrane was inferred from the density of the sample [11]. A high melt-draw ratio induced high crystallinity and density (Fig. 4b) [12]. The spinning process is a kind of quenching process, and it is difficult to experimentally detect the crystallization kinetics. However, any apprecia-

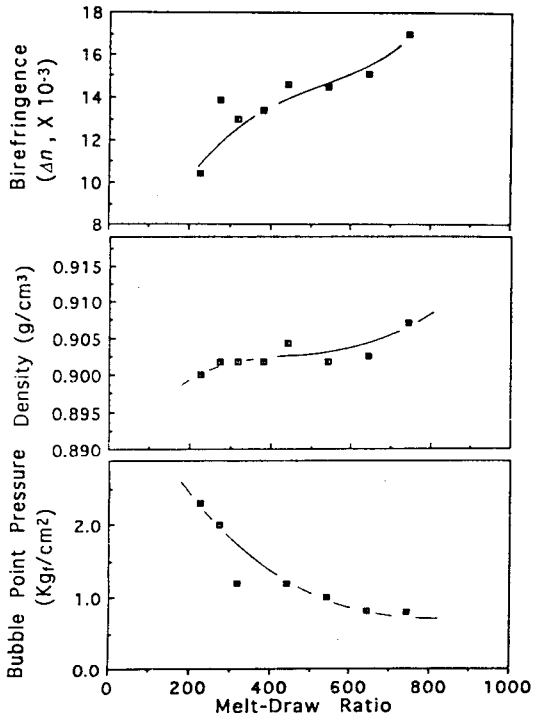

Fig. 4. Effects of melt-draw ratio on (a) birefringence, (b) density, and (c) bubble point pressure (spinning temperature, 190°C; annealing temperature, 140°C).

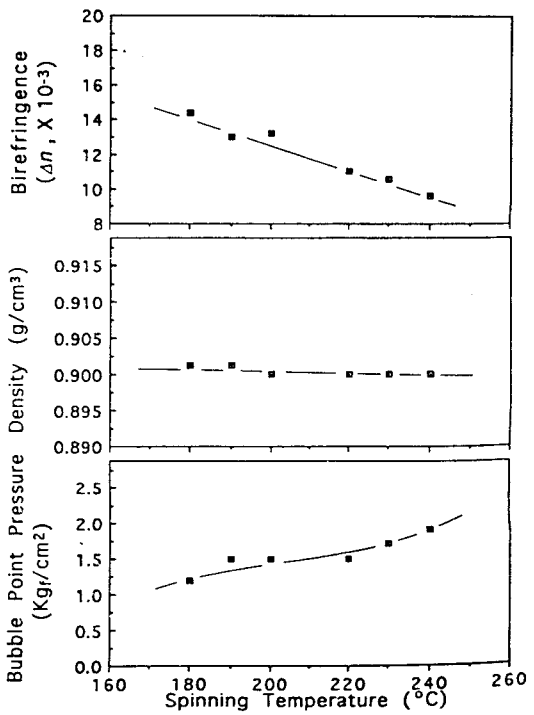

Fig. 5. Effects of spinning temperature on (a) birefringence, (b) density, and (c) bubble point pressure (melt-draw ratio, 320; annealing temperature, 140°C).

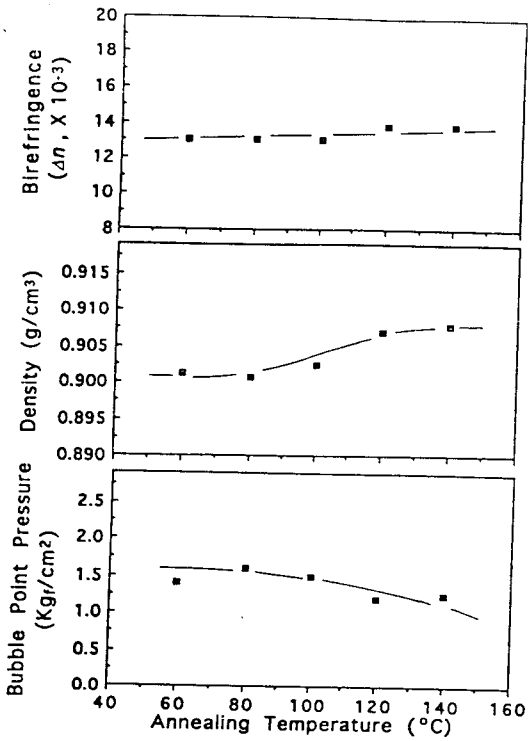

Fig. 6. Effects of annealing temperature on (a) birefringence, (b) density, and (c) bubble point pressure (melt-draw ratio, 320; spinning temperature, 190°C).

ble differences in the crystallization kinetics were not expected within the range of the spinning temperature variation in this study. Therefore, the crystallinity of the hollow fiber was not affected by the spinning temperature as shown in Fig. 5b. When the hollow fiber membrane was annealed, the crystallinity should increase due to the recrystallization and perfection of the crystalline structure by rearranging the polymer chains. As shown in Fig. 6b, the density of the hollow fiber membrane began to increase at an annealing temperature of 80°C. Temperatures below 80°C were not sufficiently high to recrystallize and perfect the crystalline structure. No further increase in density is observed above 120°C, since the membrane reached a saturation point of recrystallization and rearrangement.

The bubble point pressure depends on the melt-draw ratio, spinning temperature, and annealing temperature as shown in Figs. 4c, 5c and 6c. Since the highly melt-drawn hollow fiber is highly oriented, it should have a more ordered structure. It is probable that in a more ordered structure the amorphous phase can be more segregated from the crystalline phase, which can result in a larger pore during cold-stretching. Therefore, as the melt-draw ratio increased, the bubble point pressure decreased (or D_{max} increased). When the sample was spun at lower temperature, it should have a more ordered structure due to the higher orientation than that at higher spinning temperature. Therefore, in the same manner as the melt-draw ratio change, the bubble point pressure decreased with a decrease in spinning temperature. The annealing step also helps the hollow fiber have a more ordered structure, i.e., smaller bubble point pressure, via recrystallization and rearrangement of the polymer chain. However, the bubble point pressure was not affected by the temperature below 80°C and above 120°C as occurred in the density variation in Fig. 6b.

The scanning electron microscopic images of the inner and outer surfaces of the hollow fiber membrane (melt-draw ratio, 440; spinning temperature, 190°C; annealing temperature, 140°C) are shown in Fig. 7. The pore shape and distribution of each surface are similar, since both surfaces were formed under the same conditions. The average pore dimension was 0.3×0.1 μm in a slit shape. The maximum pore size was calculated from the bubble point pressures using Eq. (2). The surface tension of aqueous 30 vol% ethanol solution was 36.0 dyne/cm, and the contact angle between PP and the solution was 36.8°. The bubble point pressure of the membrane shown in Fig. 7 was 1.2 kg_f/cm^2, and the maximum pore diameter calculated was 0.98 μm. This is much greater than the size shown in Fig. 7.

As shown in Fig. 7, a group of neighboring micropores separated by thin fibrils formed a macro elliptic shape, which was isolated by a polymer matrix much thicker than the thin fibrils. From the scanning electron microscopic images, the pore size was obtained by averaging the size of the individual micropores separated by the thin fibrils. However, in the bubble point pressure measurement the thin fibrils seemed to be

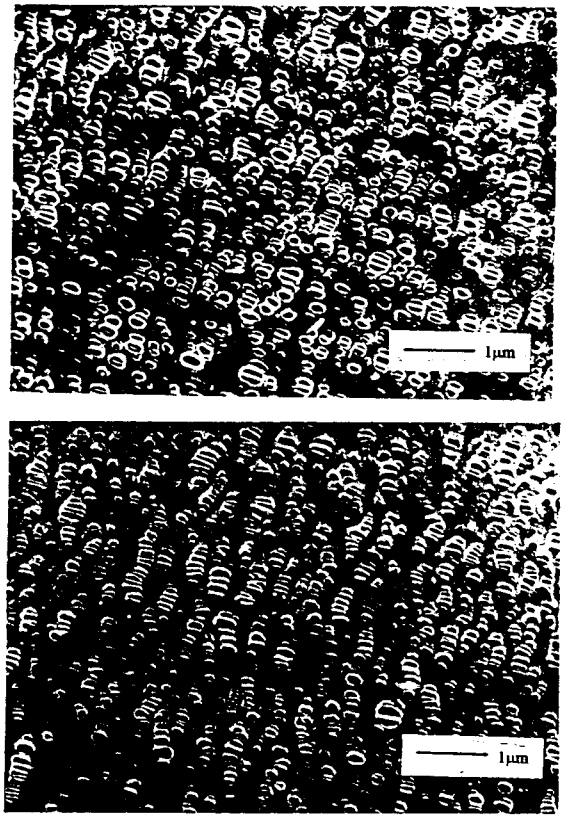

Fig. 7. SEM photographs of outer surface (top) and inner surface (bottom) of membrane.

not wetted by the medium, aqueous 30 vol% ethanol solution, in the bath. Then the macro elliptic shape formed by the group of neighboring individual micropores was considered as a single pore in that measurement. In order to confirm the wetting problem, an aqueous 40 vol% ethanol solution was used as a medium in the bath, which can better wet PP. The surface tension of aqueous 40 vol% ethanol solution was 31.5 dyne/cm, and the contact angle between PP and the solution was 23.7°. The bubble point pressure was 2.1 kg_f/cm^2, and the maximum pore diameter calculated was 0.56 μm. The variation of the maximum pore diameter by changing the medium supports the poor wetting postulation.

The pore size distribution at the outer surface calculated from the scanning electron microscopic image is plotted in Fig. 8. The average individual pore diameter was 0.1 μm, and the maximum pore diameter was 0.5 μm. The porosity of each surface was calculated as 39.0% for the outer surface and 30% for the inner surface of the membrane. All the information so far were obtained by examining the surface of the membranes. However, mercury porosimetry gives information of the complete bulk membrane, not of the surface only. A porosity of 52% was obtained from mercury porosimetry, which is much greater than that obtained of the surfaces. Therefore, the membrane prepared in this study has a greater porosity in its cross section than at its surfaces.

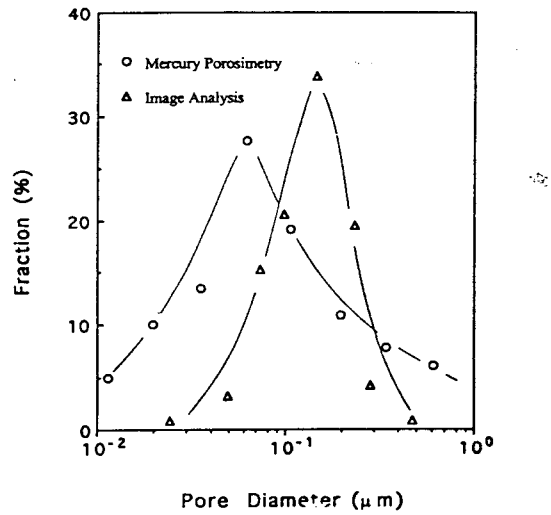

Fig. 8. Pore size distribution at the outer surface calculated by image analysis and mercury porosimetry.

The pore size distribution was also obtained from mercury porosimetry and is plotted in Fig. 8. The average pore diameter was 0.05 μm, and the maximum pore diameter was 0.6 μm. They were a little bit different from those determined by image analysis. The fiber surfaces have a different molecular morphology than the bulk, and the stretching force at the surface is different from that in the bulk, due to a different boundary condition than in the bulk. Therefore, the overall porosity is different from surface to bulk.

Microporous PP hollow fiber membranes were prepared via the MSCS process, the pore diameter of which was 0.1 to 1.0 μm. Increasing melt-draw ratio enhanced the degree of orientation, crystallinity of the hollow fibers spun, and resulted in greater maximum pore size of the membrane. Lowering the spinning temperature raised the melt viscosity inducing a higher degree of orientation of the hollow fiber and greater maximum pore size of the hollow fiber membrane. During the annealing process, the hollow fiber increased in crystallinity via recrystallization and chain rearrangement. The annealing process also helped to increase the maximum pore size of the hollow fiber membranes. A group of tiny micropores separated by thin fibrils formed a macro elliptic shape to be considered as a single pore in the bubble point pressure measurement. The discrepancy of the pore size between image analysis and mercury porosimetry came from the unclear boundary between the pore wall and the membrane surface.

membrane for plasma separation, U.S. Pat. 4,708,799 (1987).

[2] T. Ichikawa, K. Takahara, K. Shimoda, Y. Seita and M. Emi, Hollow fiber membrane and method for manufacture thereof, U.S. Pat. 4,708,800 (1987).

[3] K. Kamada, S. Minami and K. Toshida, Porous polypropylene hollow filaments and the method making the same, U.S. Pat. 4,055,696 (1977).

[4] M. Shino, T. Yamamoto, O. Fukunage and H. Yamamori, Process for making microporous polyethylene hollow fibers, U.S. Pat. 4,530,809 (1985).

[5] M.L. Druin, J.T. Loft and S.G. Plovan, Novel open-celled microporous film, U.S. Pat. 3,801,404 (1974).

[6] K. Mori, H. Fukusawa, H. Hasekawa and T. Monzen, Development and in vitro evaluation of microporous hollow fiber oxygenator, Jinkozoki, 8 (1979) 602.

[7] K. Yoshida, Structural feature and membrane properties of microporous hollow fibers, Kobunshi, 37 (1988) 142.

[8] H.S. Bierenbaum, R.B. Isaacson, M.L. Druin and S.G. Plovan, Microporous polymeric films, Ind. Eng. Chem. Prod. Res. Dev., 13 (1974) 2.

[9] A. Keller and M.J. Marchin, Oriented crystallization in polymers, J. Macromol. Sci., B1 (1967) 41.

[10] J.M. Smith (Ed.), Chemical Engineering Kinetics, McGraw-Hill, New York, 1970, p. 306.

[11] H.F. Mark (Ed.), Encyclopedia of Polymer Science and Engineering, Vol. 4, 2nd ed., Wiley, New York, 1987, p. 483.

[12] P.F. Flory, Principles of Polymer Chemistry, Cornell Univ. Press, Ithaca, NY, 1965, p. 432.